Title

Ultra-Low Loss Large Area Waveguide Coils for Integrated Optical Gyroscopes

Journal

IEEE Photonics Technology Letters, 29(2)

ISSN

1041-1135

Authors

Huffman, Taran
Davenport, Michael
Belt, Michael
et al.

Publication Date

2017-01-15

DOI

10.1109/lpt.2016.2620433

Ultra-Low Loss Large Area Waveguide Coils for Integrated Optical Gyroscopes

Taran Huffman, Michael Davenport, Michael Belt, John E. Bowers, and Daniel J. Blumenthal

***Abstract*— We discuss the design, fabrication, and measurement of a large area stitched gyroscopic coil, reporting waveguide loss, including 100 stitches over 3 m, of 0.78 dB/m and crossing loss of 0.0156 dB/crossing for a predicted ARW of 69° /hr/$\sqrt{}$Hz.**

***Index Terms*— Optical waveguides, gyroscopes.**

I. Introduction

MODERN, high-sensitivity gyroscopes are an enabling technology for a wide variety of applications including conventional navigation, control of autonomous vehicles, and geographical surveying and mapping. Interferometric optical gyroscopes (IOGs), specifically fiber optical gyroscopes (FOGS), have been demonstrated to high performance specifications beyond the most advanced MEMs gyros, but do not compare as well with respect to cost, power dissipation and size. By leveraging advanced chip-scale fabrication techniques, we can not only improve performance and manufacturability, but at the same time decrease device size, power consumption, weight, and cost. Si_3N_4 ultra-low loss waveguides (ULLWs), with losses below 0.1 dB/m loss [3], are a key component in a chip-scale gyro system, as the sensitivity of the delay coil is directly tied to the loss of the waveguide through which the optical signal propagates. We envision a fully integrated IOG with the optically active components of the source, modulator, and detector fabricated in InP/Silicon Photonic PICs bonded on top of an ULLW Si_3N_4 coil through use of a Si-interlayer, as demonstrated in [10], and similar to the work in [14].

In this letter we present the details concerning the design, fabrication, and measurement of an ULLW coil for such a device, while maintaining a manufacturing framework compatible with low loss coupling to a bonded active layer [2].

Si_3N_4 ULLWs, just as any other waveguide technology, inherently have a trade-off between optimized waveguide loss (driven by sidewall scattering) and bend radius (determined by the modal confinement within the waveguide core). Thinner waveguide cores lead to reductions in scattering loss and crossing loss, but cause the bend loss to increase [3], driven by reduced modal confinement. This relationship, combined with the fact that a gyroscope's sensitivity is proportional to its enclosed area, lead to large area coils. To this end, in this letter we stitch multiple die together to fabricate a large area ULLW gyroscope coil.

Previous waveguide based gyroscopes have utilized resonant ring waveguides (RMOGs, resonant micro-optic gyros) to amplify their sensitivity. They surpass FOGs performance in cost and size. However, they are limited in sensitivity, specifically at low rotation rates. For active RMOGs, this limit is created by the lock-in effect. Below a certain rotation threshold, feedback between the two counter propagating signals locks their phase together, so a rotation cannot be measured. In passive RMOGs coherent feedback from scatterers, facets, or simply sidewalls reduces sensitivity [5]. This is bypassed in non-resonant gyros by using ASE sources, or even swept laser sources [12]. The ultimate goal of a coil based gyroscope is to leverage the cost and size benefits of traditional waveguide based gyroscopes, without the inherent limits in sensitivity.

Other waveguide platforms have comparable loss to the Si_3N_4 ULLW platform, achieving losses below 0.1dB/m [4]. However, only the Si_3N_4 platform has other requisite components developed a delay line based gyroscope, including waveguide crossings and active integration.

II. Design

A. Coil and Waveguide

The area for our coil is determined by the area of four lithography masks. Initial calculations, following [2], indicate a large coil (∼3-10m) is optimal. The coil consists of a 3m spiral, starting at a 20mm radius and ending at an 18.75mm radius, with a waveguide spacing of 50μm, turning 25 times. The waveguide then exits the coil with straight crossings as seen in Fig. 1b). As there are 25 turns, our coil has 25 crossings spiraling in and then 25 more crossing out, for a total of 50. Additionally, this large scale device is separated into 4 lithography masks, generating 100 stitches throughout the total spiral propagation distance.

In utilizing an ULLW for large area delays for high sensitivity gyro applications, the waveguide cross-section must be carefully chosen as it significantly impacts the resulting waveguide loss, bend radius limitation, and waveguide crossing loss [3], summarized in Table I. The dimensions of the waveguide structure are given in the cross-section schematic shown in Fig, 1. The upper cladding thickness was chosen based on its impact on the mode shape with regard to bend loss and coupling to adjacent guides. The program FIMMWAVE was used to generate the mode profile, and then the interface scattering was calculated as in [3], using typical values for roughness and

Manuscript received April 12, 2016; revised September 6, 2016; accepted October 1, 2016. Date of publication October 24, 2016; date of current version January 17, 2017. This work was supported by DARPA MTO under iWOG Contract HR0011-14-C-0111.

The authors are with the Department of Electrical and Computer Engineering, University of California at Santa Barbara, Santa Barbara, CA 93106 USA.

Color versions of one or more of the figures in this letter are available online at http://ieeexplore.ieee.org.

Digital Object Identifier 10.1109/LPT.2016.2620433

TABLE I
CORE THICKNESS AND PROPAGATION

Core Thickness (nm)	Scattering Loss (dB/m)	Bend Limit (mm)
40	0.26 (simulated)	11
60	3	3
90	6	1
175	15	.5

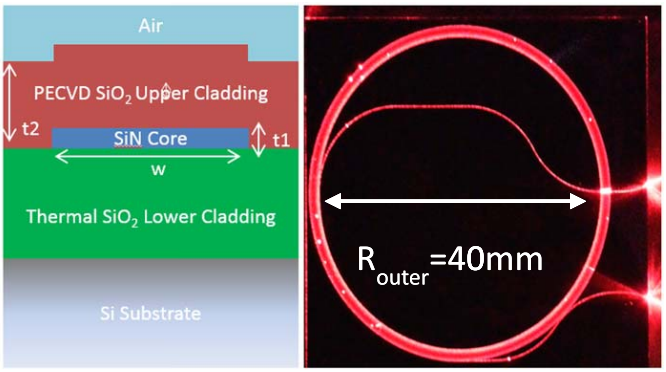

a) b)

Fig. 1. A cross section of the waveguide geometry and an overhead view of the fabricated coil illuminated with a red laser (wavelength of 650 nm), measuring 50mm by 42mm in entirety. The waveguide geometry for the coil has t1 = 40nm, w = 7μm, and t2 = 5μm. The schematic diagram is not to scale.

correlation length for the surface and sidewall roughness, 0.1nm and 3nm respectively. The scattering calculation estimates 0.26dB/m loss.

A large polarization extinction is desired between modes to minimize nonreciprocities in the coil [5]. The high aspect ratio waveguides create modal size differences between TE and TM light, causing TM light to have much greater bend loss [3]. By including several bends near the TE bend limit, we can extinguish the TM light and create a large extinction between the TE and TM modes.

B. Crossings

The crossings can be evaluated as straight-straight crossings, as the radius is large enough that it introduces a perturbation to the mode on the order of 10^{-6} change in the effective index. An image of the crossing is shown in Fig. 2. Simulating these crossings in Lumerical FDTD yields a crossing loss of 0.02dB/crossing. Over the 50 crossings this generates an estimated 1dB of loss.

C. Stitches

A stitch in a waveguide is produced when the edges of two die meet on a wafer. The die alignment is not perfect, and an offset is produced, shown in Fig. 3. Tests of the lithographic alignment yield a stitching error of 50nm. This is consistent with the alignment accuracy reported for our stepper. This represents a much smaller perturbation than a waveguide crossing, so we expect the loss and reflection of a stitch to be negligible. Stitches with a 50, 100, and 150nm offset were simulated in Lumerical FDTD. The simulations yielded, respectively, 0.006, 0.011, and 0.016dB of loss per stitch.

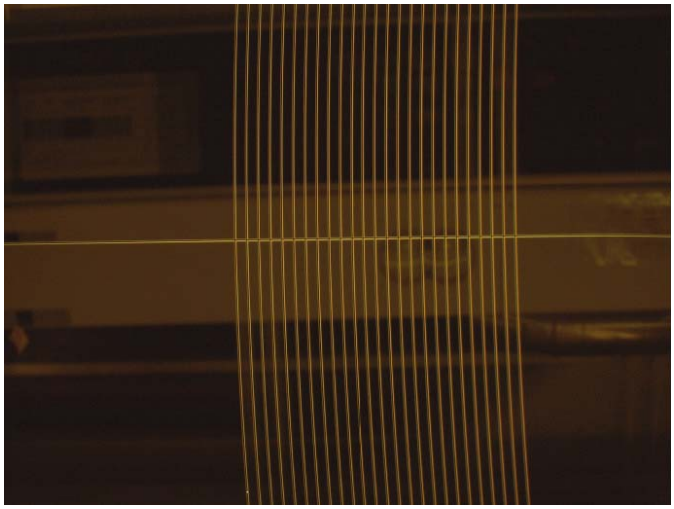

Fig. 2. A dark field optical image of the crossings, with reflected clean room equipment slightly visible in the background. This image was taken during processing and is of the exposed etched core.

III. FABRICATION

Processing begins with the growth of 15μm of thermal SiO_2 for the lower cladding on a 0.5mm thick 100mm diameter silicon wafer. The Si_3N_4 core is then deposited using low pressure chemical vapor deposition (LPCVD), performed by Rogue Valley Microdevices. We use an ASML PAS 5500 DUV stepper to define the core with 4 separate masks exposed in succession. The core is then dry etched with a CHF_3, CF_4, and O_2 mixture. After cleaning and inspection optically and with SEM, the SiO_2 upper cladding is deposited with plasma enhanced chemical vapor deposition (PECVD) at 300 °C. The entire wafer is then annealed in an oxygen environment, for 7 hours at 1050 °C. The upper cladding deposition and anneal are performed twice, leading to a total of 5μms of upper cladding. The coil is then diced and tested.

IV. RESULTS

A. Waveguides

Due to their low loss, the widely used cutback technique cannot be utilized, as the facet coupling non-uniformity due to device dicing is larger than the magnitude of loss itself for most reasonably sized test structures. Thus, we leverage a waveguide loss measurement technique based on optical backscattered reflectometry (OBR). A full description of this type of measurement and analysis is given in [3]. In the case of the large area stitched coil, this measurement will include the stitches, crossings, and additional scatterers in the measurement. Such a trace is shown in Fig. 4, for both TE and TM polarizations. The TM light experiences much higher loss and is essentially eliminated tens of centimeters into the coil, the remaining noise floor is the TE light that wasn't eliminated by the polarization rotator. There is a 25dB extinction between the two modes after less than 50cm of propagation.

Fitting a slope to the TE plot in Fig. 4, yields the wavelength dependent loss, shown in Fig. 5. The increased loss at lower wavelengths is due to the hydrogen present from the PECVD oxide [9]. At higher wavelengths the curve flattens, which our model indicates is a result of scattering loss.

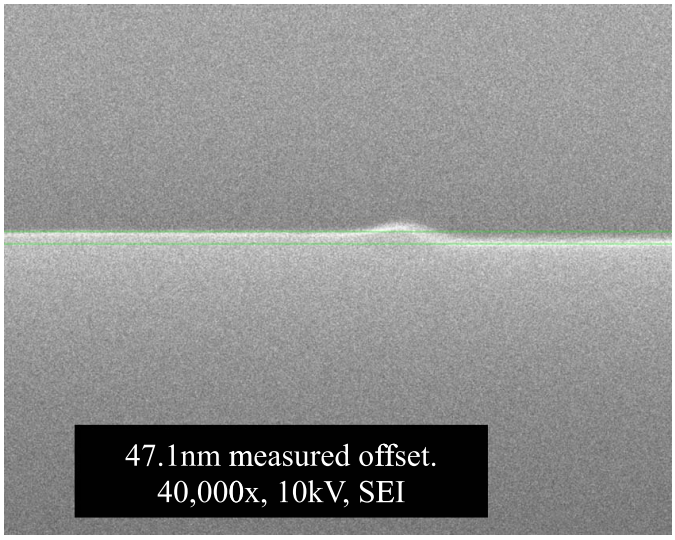

Fig. 3. An SEM image of the stitch on a 7um wide, 40nm thick waveguide. The green bars on the image specify the measured 47.1nm offset.

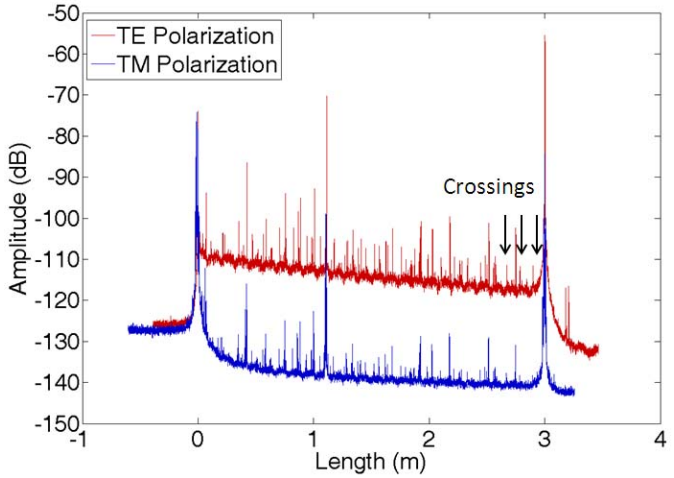

Fig. 4. OBR trace for the large area coil. Besides the facets, all of the largest reflections (such as the ones found near z = 0.5 m and z = 1.1 m) are the result of discrete impurities, which act as optical scatterers.

Taking the crossing loss result from the next section, we can separate the crossing loss from the waveguide propagation data, to effectively reduce the loss at all wavelengths by 0.26dB/m. Such a subtraction gives us a lowest-case propagation loss 0.78dB/m at 1595nm. It is important to keep in mind that this value still includes the loss incurred by the DUV reticle stitching process. Over the 3 meters of the coil the waveguide, stitching, and other miscellaneous scatterers contribute a total of 2.34dB of loss.

This method can't be used to measure the propagation loss of the TM mode, as it is lost too quickly to be separated from the reflection peak. A through measurement of the coil yields a 35 dB difference in power for the TM and TE modes, which is the extinction limit for the polarization rotator used.

B. Crossings

The waveguide crossing loss was measured on a separate set of test structures located on the same processed wafer

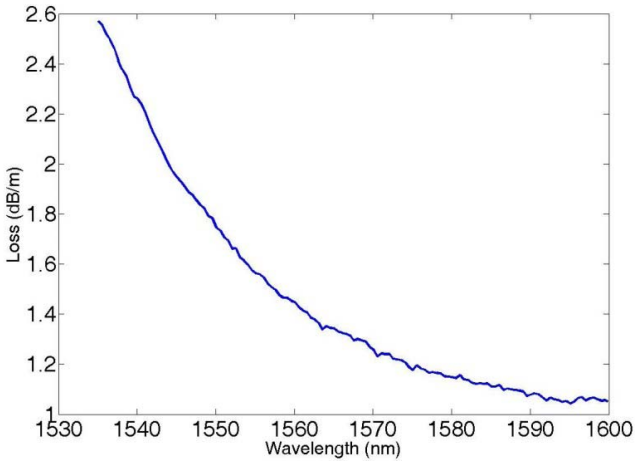

Fig. 5. Wavelength dependent loss of the large area coil.

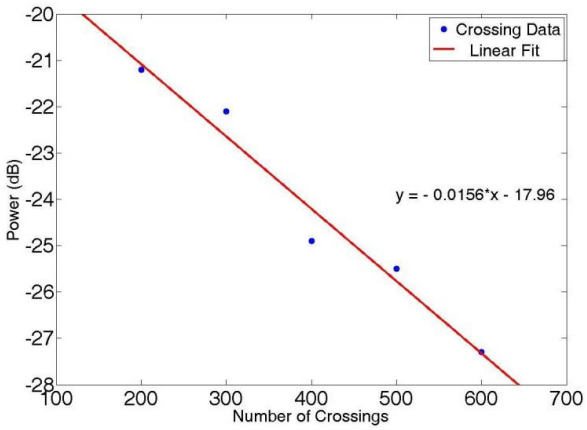

Fig. 6. Crossing test structure data. The R^2 of the fit is 0.97.

as the waveguide coil. Here we employed adjacent straight waveguides with varying numbers of waveguide crossings to simulate the cutback method of measurement. A linear fit is then performed to extract the loss per crossing.

From Fig. 6, we can extract the crossing loss as 0.0156dB/crossing, close to our simulated value of 0.02dB/crossing. We can calculate the total penalty generated from crossings found within our stitched delay coil. Counting the 50 crosses of the entire coil, we have a crossing penalty of 0.78dB.

C. Stitches

FDTD simulations predict a 0.006dB loss per stitch with a 50nm offset. A similar cut-back style structure such as the one used for the waveguide crossings is impossible as the minimum stitching length is 1mm, a limit of the stepper, and the structure would require several hundreds of stitches.

Instead we turn to our waveguide loss measurements and simulations. The highest our stitching loss could conceivably be is 0.023 dB/stitch, if we were to assume the waveguide is otherwise loss-less. If instead we take our waveguide loss to be equal to our simulation value, we find our stitching loss to be 0.016 dB/stitch. Considering this value is slightly larger than our crossing loss, which represents a much greater perturbation

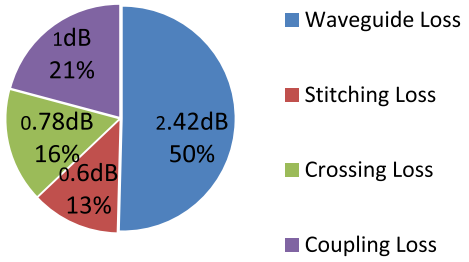

Fig. 7. Contributions of different loss sources.

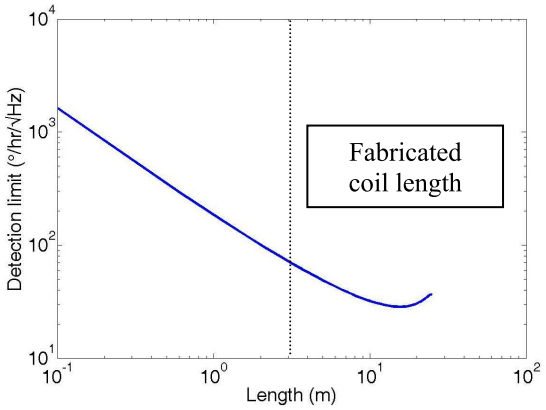

Fig. 8. Theoretical coil detection limit vs. length.

to the propagating light, it is probable the stitching simulation is much more accurate than the waveguide scattering simulation, and that the value is closer to 0.006dB. This is additionally supported by the accuracy of the crossing loss simulation and the fact that the stitches are not visible in the OBR trace.

V. Discussion

The total loss of the coil is 4.8dB, taking into account waveguide, stitching, crossing, and coupling loss, which have been separated as in Fig. 7.

The ultimate evaluation of the coil is how it performs as a rotation sensor. We evaluate this using the calculation described in [2]], shown in Fig. 8. We assume an ASE source with 100mW of optical power before being coupled to the coil, with a RIN of -128dBc/Hz.

The coil's current length allows for an angle random walk (ARW) of 69° /hr/$\sqrt{}$Hz. From the plot it is seen that our coil is quite short and the sensitivity can be improved greatly by increasing the length of the coil. The optimum ARW is 28° /hr/$\sqrt{}$Hz and occurs at 15m.

State of the art RMOGs can theoretically achieve on the order of 10° /hr/$\sqrt{}$Hz [13], [15], with a smaller footprint. For comparison, we calculated the sensitivity of a coil with state of the art loss of 0.1dB/m, and use the maximum length with the same footprint of 30 meters. This results in an ARW of 8.5° /hr/$\sqrt{}$Hz. To improve upon this value further requires increasing the length within the same footprint.

VI. Conclusion

We reviewed the design and characterization of a large area gyroscopic coil. We measured a crossing loss of 0.0156dB/crossing in close agreement to simulations. The waveguide and stitching loss prove very difficult to separate, but sum together to give 0.78dB/m with 100 crossings over 3 meters. It seems very likely that the stitching loss is close to the simulated value of 0.006dB/stitch and the waveguide loss is near 0.58dB/m. These values taken together yield a predicted ARW of 69°/hr/$\sqrt{}$Hz.

As the length of the coil increases, the inner radius of the spiral structure is reduced and this reduces the effectiveness of the coil. As future work, this reduction could be combated with multiple waveguide layers, allowing for increased length and maximizing the area of the coil. Low loss and broadband vertical couplers have been demonstrated with this platform [9].

Acknowledgements

The views and conclusions contained in this document are those of the authors and should not be interpreted as representing official policies of the Defense Advanced Research Projects Agency or the U.S. Government.

References

[1] R. Lutwak, "Micro-technology for positioning, navigation, and timing towards PNT everywhere and always," in *Proc. Int. Symp. Inertial Sensors Syst. (ISISS)*, Feb. 2014, pp. 1–4.
[2] S. Srinivasan *et al.*, "Design of integrated hybrid silicon waveguide optical gyroscope," *Opt. Exp.*, vol. 22, no. 21, pp. 24988–24993, 2014.
[3] J. F. Baters *et al.*, "Ultra-low-loss high-aspect-ratio Si_3N_4 waveguides," *Opt. Exp.*, vol. 19, no. 4, pp. 1363–1374, 2011.
[4] H. Lee, T. Chen, J. Li, O. Painter, and K. J. Vahala, "Ultra-low-loss optical delay line on a silicon chip," *Nature Commun.*, vol. 3, May 2012, Art. no. 867.
[5] C. H. Lefevre, *The Fiber-Optic Gyroscope*. Norwood, MA, USA: Artech House, 2014.
[6] M. N. Armenise, *Advances in Gyroscope Technologies*. Springer, 2010.
[7] Z. Jin, X. Yu, and H. Ma, "Closed-loop resonant fiber optic gyro with an improved digital serrodyne modulation," *Opt. Exp.*, vol. 21, no. 22, pp. 26578–26588, 2013.
[8] R. A. Bergh, H. C. Lefevre, and H. J. Shaw, "All-single-mode fiber-optic gyroscope with long-term stability," *Opt. Lett.*, vol. 6, no. 10, pp. 502–504, 1981.
[9] S. C. Mao *et al.*, "Low propagation loss SiN optical waveguide prepared by optimal low-hydrogen module," *Opt. Exp.*, vol. 16, no. 25, pp. 20809–20816, 2008.
[10] H. Park *et al.*, "Hybrid silicon evanescent laser fabricated with a silicon waveguide and III-V offset quantum wells," *Opt. Exp.*, vol. 13, no. 23, pp. 9460–9464, 2005.
[11] R. Moreira *et al.*, "Optical interconnect for 3D integration of ultra-low loss planar lightwave circuits," in *Proc. Adv. Photon.*, 2013, p. IT2A.
[12] T. Komljenovic *et al.*, "Frequency modulated lasers for interferometric optical gyroscopes," *Opt. Lett.*, vol. 41, no. 8, pp. 1773–1776, 2016.
[13] C. Ciminelli *et al.*, "High performance InP ring resonator for new generation monolithically integrated optical gyroscopes," *Opt. Exp.*, vol. 21, no. 1, pp. 556–564, 2013.
[14] S. Gundavarapu *et al.*, "Design of integrated hybrid silicon waveguide optical gyroscope," in *Proc. Opt. Fiber Commun. Conf., Tech. (OSA)*, Mar. 2016, paper W4E.5.
[15] C. Ciminelli, F. Dell'Olio, C. E. Campanella, and M. N. Armenise, "Numerical and experimental investigation of an optical high-Q spiral resonator gyroscope," in *Proc. ICTON*, Jul. 2012, pp. 1–4.